PIKfyve inhibition blocks endolysosomal escape of α-synuclein fibrils and spread of α-synuclein aggregation

AUTHORS:

Stephanie K. See[1,2], Merissa Chen[1], Sophie Bax[3], Ruilin Tian[1,4], Amanda Woerman[5], Eric Tse[1], Isabel E. Johnson[6], Carlos Nowotny[6], Elise N. Muñoz[6], Janine Sengstack[6], Daniel R. Southworth[6,7], Jason E. Gestwicki[1,8], Manuel D. Leonetti[3], Martin Kampmann[1,3,7,*]

AFFILIATIONS:

[1]Institute for Neurodegenerative Diseases, University of California, San Francisco, San Francisco, CA 94158

[2]Graduate Program in Chemistry and Chemical Biology, University of California, San Francisco, San Francisco, CA 94158

[3]Chan Zuckerberg Biohub, San Francisco, California 94158

[4]Biophysics Graduate Program, University of California, San Francisco, San Francisco, CA 94158

[5]Institute for Applied Life Sciences and Department of Biology, University of Massachusetts, Amherst, Massachusetts 01003

[6]Tetrad Graduate Program, University of California, San Francisco, San Francisco, CA 94158

[7]Department of Biochemistry and Biophysics, University of California, San Francisco, San Francisco, CA 94158

[8]Department of Pharmaceutical Chemistry, University of California, San Francisco, San Francisco, CA 94158

*Corresponding author

ABSTRACT

The inter-cellular prion-like propagation of α-synuclein aggregation is emerging as an important mechanism driving the progression of neurodegenerative diseases including Parkinson's disease and multiple system atrophy (MSA). To discover therapeutic strategies reducing the spread of α-synuclein aggregation, we performed a genome-wide CRISPR interference screen in a human cell-based model. We discovered that inhibiting PIKfyve dramatically reduced α-synuclein aggregation induced with both recombinant α-synuclein fibrils and fibrils isolated from MSA patient brain. While PIKfyve inhibition did not affect fibril uptake or α-synuclein clearance or secretion, it reduced α-synuclein trafficking from the early endosome to the lysosome, thereby limiting fibril escape from the lysosome and reducing the amount of fibrils that reach cytosolic α-synuclein to induce aggregation. These findings point to the endolysosomal transport of fibrils as a critical step in the propagation of α-synuclein aggregation and a potential therapeutic target.

INTRODUCTION

Neurodegenerative diseases are a pressing global public health challenge due to the lack of disease-modifying therapies. A major reason for the absence of effective treatments is likely our incomplete understanding of the molecular and cellular mechanisms underlying disease progression. A major advance in neurodegeneration research was the discovery that scrapie, an infectious neurodegenerative disease, is caused by the spread of protein aggregates via their prion forms.[1] Prion proteins can template the conversion of healthy native proteins into an aggregated conformer that in turn continues to propagate. Since the discovery of prions, numerous independent studies suggest that the prion-like propagation of specific neuronal proteins such as tau and α-synuclein drive noninfectious neurodegenerative diseases such as Alzheimer's disease or Parkinson's disease.[2–4] Our understanding of the mechanisms that control the prion-like spread of these proteins is incomplete. Fully elucidating these mechanisms systematically will further our understanding of disease progression and provide new therapeutic targets.

Here, we investigate the mechanisms underlying the prion-like spreading of α-synuclein aggregation with the goal to pinpoint potential therapeutic targets to inhibit this process. α-synuclein aggregation is a common hallmark of Parkinson's disease, and is strongly correlated with neuronal death and subsequent cognitive and motor dysfunction.[5] Copy number variations or point mutations in the α-synuclein gene have been linked to familial Parkinson's Disease.[5] α-synuclein aggregation occurs in other neurodegenerative diseases, broadly categorized as synucleinopathies, including multiple systems atrophy (MSA).[5]

α-synuclein aggregation and propagation can be modeled in cultured HEK293T cells that express fluorescently tagged versions of α-synuclein harboring patient-derived point mutations.[6–8] In this system, addition of α-synuclein fibrils to the culture medium triggers the conversion of diffuse soluble α-synuclein into aggregated puncta. This cell-based model has enabled the characterization of α-synuclein species with seeding activity from post-mortem patient brains, further validating the physiological relevance of these cell-based models.[9–11]

These biosensors and others[12] have been instrumental in detecting seeding activity of α-synuclein preparations. Importantly, cell-based models can also be used to discover new pathways that control propagation of α-synuclein aggregation. While previous studies sought to define the mechanisms of α-synuclein toxicity in yeast[13,14] and mechanisms that regulate levels of α-synuclein in mammalian cells[15–17], cellular pathways that control propagation of α-synuclein aggregation in mammalian cells have not been systematically characterized. We hypothesized that such pathways could encompass those that control uptake of α-synuclein fibrils, trafficking of fibrils through the endolysosomal system and escape to the cytosol, templated aggregation of soluble α-synuclein, and aggregate clearance (**Fig. 1A**).

In order to discover cellular pathways that control spreading of α-synuclein aggregation, we applied our CRISPR interference-based (CRISPRi) genetic screening platform[18,19] to a fluorescence resonance energy transfer (FRET) based model of α-synuclein aggregation in mammalian cells. Using this approach, we identified the phosphotidylinositol pathway as a critical regulator of the spreading of α-synuclein aggregation. Inhibition of the synthesis of multiple phosphatidylinositol species lowered aggregation. Specifically, inhibition of the kinase PIKfyve dramatically reduced α-synuclein trafficking through the endolysosomal system, thereby limiting the escape of α-synuclein seeds from lysosomal compartments and slowing subsequent templating of α-synuclein aggregation in the cytosol. These discoveries define

88 mechanisms of α-synuclein trafficking that can be inhibited pharmacologically to reduce
89 aggregation, highlighting their potential as therapeutic targets.
90
91
92 **RESULTS**
93
94 **Cell-based model of prion-like propagation of α-synuclein aggregation**
95
96 In order to identify cellular factors that control the prion-like propagation of α-synuclein
97 aggregation (**Fig. 1A**), we established a cell-based model with a FRET readout. A similar FRET-
98 based model had been previously developed by the Diamond Lab to monitor aggregation by
99 microscopy and flow cytometry.[9] Given the different aggregation propensities of wild-type α-
100 synuclein and the Parkinson's disease-associated A53T and E46K point mutations, we generated
101 three versions of this cell-based system: wild-type, A53T and E46K.
102 First, we generated recombinant α-synuclein fibrils to serve as aggregation seeds. We
103 purified monomeric human α-synuclein from *Escherichia coli* and induced fibrillization by
104 vigorous agitation at 37 ºC. We verified the generation of amyloid fibrils by the increase in
105 Thioflavin T fluorescence (**Fig. 1B**) and negative stain EM (**Fig. 1C**). These fibrils were
106 subsequently sonicated into smaller seeds.
107 Next, we co-expressed two versions of full-length human α-synuclein fused to the
108 fluorescent proteins mClover2 and mRuby2, respectively, in HEK293T cells. We reasoned that
109 upon triggering aggregation with α-synuclein fibrils added to the cells, the monomeric fusion
110 proteins would come within close proximity to each other and generate a detectable FRET signal
111 (**Fig. 1D**).
112 Fluorescent constructs were stably introduced to HEK293T cells by lentivirus. We then
113 selected monoclonal lines based on high expression of the fusion proteins and dynamic range of
114 the FRET signal. In the absence of fibrils, these reporter cells showed diffuse intracellular
115 fluorescence without visible aggregates when monitored by fluorescence microscopy (**Fig. 1E**)
116 and appeared as a single population when FRET levels were monitored by flow cytometry (**Fig.
117 1F**). Upon exposure to recombinant α-synuclein fibrils complexed with lipofectamine, we
118 observed that the fluorescent reporter constructs formed visible puncta by fluorescent
119 microscopy (**Fig. 1E**), and a second distinct FRET-positive population of cells emerged by flow
120 cytometry (**Fig. 1F**), indicating aggregation of the intracellular α-synuclein constructs. We found
121 that all three fibril types triggered aggregation in a dose-dependent manner when added to cell
122 types expressing the reporters with the corresponding sequences (WT, A53T or E46K), as
123 quantified by the percentage of FRET-positive cells (**Fig. 1G**). The E46K α-synuclein FRET
124 reporter line reproducibly generated the highest percentage of FRET-positive cells, and
125 generated detergent and urea resistant aggregates (**Fig. 1H**), making it an ideal cell line to use in
126 a genome-wide genetic screen to identify cellular factors controlling α-synuclein aggregation.
127
128 **Genome-wide screen for modifiers of prion-like propagation of α-synuclein aggregation**
129
130 To enable a genetic screen for modifiers of propagation of α-synuclein aggregation, the
131 cell lines described above also expressed catalytically inactive Cas9-BFP-KRAB (dCas9-BFP-
132 KRAB) fusion protein. dCas9-BFP-KRAB can be directed by single guide RNAs (sgRNAs) to

133 knock down a specific gene of interest,[20] enabling large-scale genetic screens in mammalian
134 cells.[18]

135   The screening strategy is illustrated in **Figure 2A**. We transduced these cells with pooled
136 lentiviral libraries containing sgRNAs targeting every protein-coding gene in the genome and
137 nontargeting control sgRNAs. Cells transduced with sgRNAs were exposed to recombinant α-
138 synuclein fibrils at concentrations that yielded the half-maximal percentage of FRET-positive
139 cells, thereby maximizing the dynamic range for detecting cellular factors that either increase or
140 decrease α-synuclein aggregation. FRET-negative and FRET-positive cell populations were
141 separated by FACS. Sufficient numbers of cells were collected from each population to achieve
142 at least 500x average representation of cells per sgRNA elements in the library. Genomic DNA
143 was isolated, sgRNAs were PCR-amplified, and frequencies for each sgRNA in each population
144 were quantified by next-generation sequencing. We evaluated the effect of gene knockdown on
145 the formation of α-synuclein aggregates using our previously described bioinformatics
146 pipeline.[18,21–23]

147   The genome-wide screen uncovered genes knockdown of which either increased or
148 decreased α-synuclein aggregation (**Table S1**). Many of the top hits could be assigned to one of
149 the following biological categories: Endolysosomal system / vesicular trafficking, cytoskeleton,
150 gene expression, mitochondria, nucleocytosolic transport (**Fig. 2B, Table S1**).

151   Next, we selected hits from the primary genome-wide screen, which was performed with
152 the α-synuclein (E46K) FRET-reporter, for further characterization in secondary screens. These
153 hits were first selected from genes with an FDR < 0.1 and further narrowed to exclude heavily
154 redundant genes specific to a biological pathway, resulting in a focused library targeting 249
155 genes (**Table S2**). Using this focused library, we conducted secondary screens with all three
156 versions of the α-synuclein reporter. The hits targeted by this focused retest library revalidated in
157 all three cell lines robustly with minimal differences between the α-synuclein variants (**Fig. 3A,**
158 **Fig. S1, Table S2**).

159   Genes that reproduced strongly in the WT, A53T, and E46K cell lines are displayed in
160 **Figure 3B**, grouped by their biological pathways. The knockdown of many genes in the
161 endolysosomal system dramatically reduced aggregation. One major pathway stood out for its
162 strong impact on α-synuclein aggregation: the phosphatidylinositol pathway, a major signaling
163 pathway that regulates, among other processes, endolysosomal trafficking and autophagy. We
164 decided to prioritize this pathway for further characterization because knockdown of several
165 factors in this pathway robustly reduced aggregation, making it a potential therapeutic target.
166
167

168 **Pharmacological inhibition of PIKfyve and other phosphatidylinositol kinases reduces α-**
169 **synuclein aggregation**
170

171   In order to comprehensively test which members of the phosphatidylinositol pathway
172 control aggregation, we selected a panel of small molecule inhibitors of major kinases involved
173 in this pathway (**Fig. 4A, Fig. S2**). Interestingly, the majority of these inhibitors blocked
174 aggregation robustly (**Fig. 4A**). In particular, apilimod, an inhibitor of PI-3P-5-kinase (PIKfyve),
175 which phosphorylates the D-5 position in phosphatidylinositol-3-phosphate (PI3P) to yield
176 phosphatidylinositol 3,5-bisphosphate (PI(3,5)P2),[24] dramatically reduced aggregation with IC_{50}
177 values below 25 nM (**Fig. 4B**). To confirm these results genetically, we cloned two individual
178 sgRNAs each targeting PIKfyve and validated that PIKfyve knockdown in our FRET reporter

4

179 lines also reduced aggregation (**Fig. 4C**, **Table S2**) but to a lesser extent compared to the
180 pharmacological inhibitors. PIKfyve inhibition also reduced the amount of insoluble α-synuclein,
181 measured by a filter trap assay, in a dose-dependent manner (**Fig. 4D,E**).
182   Recently, α-synuclein fibrils isolated from post-mortem brains from patients with a
183 synucleinopathy called multiple system atrophy (MSA) were shown to trigger aggregation in
184 cellular and mouse models of α-synuclein propagation.[6,9,10] We tested the effect of PIKFyve
185 inhibition on α-synuclein aggregation triggered by α-synuclein fibrils isolated from deceased
186 MSA patient brain samples. We found that PIKYVE inhibition decreased α-synuclein
187 aggregation in our FRET reporter line seeded with patient brain-derived α-synuclein by flow
188 cytometry (**Fig. 4F**).
189
190 **PIKfyve inhibition does not increase autophagic flux, α-synuclein secretion, nor decrease**
191 **fibril uptake**
192
193   We next investigated the mechanism by which PIKfyve inhibition reduces α-synuclein
194 aggregation. Given the importance of autophagy for the clearance of aggregated proteins,
195 including α-synuclein,[25] we hypothesized that PIKfyve might reduce aggregation by increasing
196 autophagic flux. We first evaluated the effect of PIKfyve inhibition on autophagy using a LC3
197 cell-based reporter. This reporter consists of a fusion construct of GFP-LC3 and RFP-LC3ΔG
198 that is cleaved by ATG4 during autophagy. GFP-LC3 is degraded by autophagy whereas RFP-
199 LC3ΔG remains in the cytosol as an internal control. Autophagic flux can then be quantified by
200 flow cytometry as the ratio of RFP to GFP.[26] Surprisingly, we discovered that PIKfyve inhibition
201 decreased, rather than increased autophagic flux (**Fig. 5A**) in the presence of torin, a
202 pharmacological activator of autophagy.
203   Previous studies have suggested that the inhibition of autophagy can promote the
204 exocytosis of α-synuclein as an alternative clearance mechanism.[27] We therefore hypothesized
205 that PIKfyve inhibition may lower levels of aggregated α-synuclein by promoting export of
206 intracellular α-synuclein. To test this hypothesis, we performed an ELISA to detect the level of
207 α-synuclein-Clover in the cell culture media after triggering aggregation (**Fig. 5B**). PIKfyve
208 inhibition did not cause an increase in the amount of α-synuclein-Clover in the media, and there
209 was no decrease in intracellular α-synuclein-Clover levels (**Fig. 5C**), suggesting that an export
210 mechanism could not explain the dramatic decrease in aggregation during PIKfyve inhibition.
211   We then evaluated if PIKFyve inhibition reduced aggregation by blocking the initial fibril
212 uptake into cells. By measuring the uptake of fluorescently tagged fibrils at different apilimod
213 concentrations, we determined that PIKFyve inhibition did not alter fibril uptake (**Fig. 5D**).
214
215 **PIKfyve inhibition interferes with α-synuclein fibril trafficking to the lysosome and**
216 **lysosomal rupture**
217
218   Given the role of PIKfyve at multiple stages of the endolysosomal pathway,[28] we sought
219 to investigate if PIKfyve inhibition could alter fibril trafficking. We monitored fibril transport in
220 relationship to the early endosome marker EEA1 (**Fig. 6A**) and the late endosome/lysosome
221 marker LAMP1 (**Fig. 6B**) at 30 min, 1 h, 2h, 4h, and 24 h after fibril exposure. In the absence of
222 PIKfyve inhibition, fibrils are not detected in EEA1-positive compartments at these time points
223 (**Fig. 6A**), but accumulate in LAMP1-positive compartments as early as 30 min after fibril
224 exposure (**Fig. 6B**). In the presence of apilimod, which resulted in enlargement of both EEA1

225   and LAMP1 vesicles, fibrils colocalized with EEA1 vesicles at the 1-hour timepoint,
226   dramatically reducing the number of fibrils that reach LAMP1 vesicles at early and late
227   timepoints. These results suggest that PIKfyve inhibition reduces fibril trafficking from the early
228   to late endosome/lysosome.
229   α-synuclein fibrils have been previously shown to cause endolysosomal damage,[29]
230   leading us to hypothesize that PIKFyve inhibition may reduce α-synuclein aggregation by
231   reducing fibril-induced rupture of the lysosome and subsequent escape of fibrils to the cytosol.
232   We tested this hypothesis by monitoring the formation lysosomal damage using a cytosolic GFP
233   fusion of galectin 3 (GAL3), a lectin that binds β-galactosides and forms puncta when these
234   sugars are exposed on damaged endolysosomes.[30] Consistent with previously reported studies[29]
235   α-synuclein fibrils caused endolysomal damage. Pharmacological and genetic PIKFyve
236   inhibition dramatically reduced α-synuclein fibril-induced endolysomal damage (**Fig. 7A-C**).
237   Given the strong reduction of lysosomal damage upon PIKFYVE inhibition, we asked
238   whether PIKFyve inhibition generally protects lysosomes from damage, or whether the effect is
239   specific to damage induced by α-synuclein fibrils. To address this question, we treated cells with
240   leucyl-leucyl-*O*-methyl ester (LLOME), a compound that accumulates in the lumen of acidified
241   organelles, rapidly forms membranolytic polymers after cleavage by cathepsin C,[30,31] thereby
242   causing direct lysosomal rupture. We confirmed that LLOME damages endolysosomal
243   membranes in our cell line using the GAL3-GFP reporter (**Fig. 7D**). Apilimod did not protect
244   cells from LLOME-induced lysosomal damage, but rather sensitized them (**Fig. 7D**), indicating
245   that its protective effect in the presence of α-synuclein fibrils is due to inhibition of fibrils
246   reaching the lysosome, as opposed to a direct effect on lysosomal integrity.
247   These results together suggest that PIKfyve controls fibril trafficking from the early to
248   late endosome, and that the inhibition of PIKfyve decreases the amount of fibrils reaching
249   lysosomes. The resulting lysosomal rupture limits fibrils from templating aggregation of soluble
250   α-synuclein in the cytosol, inhibiting α-synuclein aggregate spreading (**Fig. 8**).

251
252
253   **DISCUSSION**
254
255   We used our CRISPRi-based genetic screening platform to discover new mechanisms
256   controlling prion-like spreading of α-synuclein aggregation in a cell-based model, and potential
257   therapeutic targets to block this process. Importantly, we discovered that the inhibition of
258   PIKfyve decrease aggregation by blocking fibril trafficking to lysosomes, thereby decreasing the
259   endolysosomal escape of α-synuclein fibrils.
260   Since our observations were made in an *in-vitro* model of α-synuclein aggregation, it
261   remains to be tested whether inhibition of PIKfyve may reduce spread and propagation of α-
262   synuclein in the context of neurodegenerative diseases *in vivo*. Beyond its potential to reduce
263   prion-like spreading of protein aggregation, inhibition of PIKfyve has been shown to have other
264   beneficial effects in neurodegeneration as well. The inhibition of PIKfye has been shown to be
265   beneficial in mouse models of amyotrophic lateral sclerosis and frontotemporal dementia
266   induced by repeat expansions in C9orf72 by reversing endolysosomal defects.[32]
267   Intriguingly, PIKfyve inhibition has been shown to block infection with SARS-CoV-2 *in*
268   *vitro*, likely by a mechanism similar to the one we have delineated here for α-synuclein fibrils[33].
269   Apilimod is currently evaluated in a clinical trial for efficacy in COVID-19 patients
270   (NCT04446377). This suggests that PIKfyve inhibition can block endolysosomal trafficking of

6

271   both pathogenic protein aggregates and viruses, and effective inhibitors could have a broad
272   spectrum of clinical uses.

273   Our genome-wide screen also pointed to additional pathways relevant for prion-like
274   propagation of α-synuclein aggregation, including other trafficking factors, such as the
275   Parkinson's risk gene DNAJC13. Another major class of hits is related to gene expression
276   (including translation and ribosome biogenesis). These hits, however, may be pleiotropic as they
277   likely affect expression of many genes.

278   We had expected to discover a larger network of molecular chaperones that regulate α-
279   synuclein aggregation. Numerous *in vitro* and *in vivo* studies point to chaperones and their co-
280   chaperones that strongly control aggregation and may be important therapeutic targets for
281   synucleinopathies.[34,35] The knockdown of individual chaperones did not have a major impact on
282   α-synuclein aggregation in our genetic screen. This could be due to the redundancy of molecular
283   chaperones in cells and would be better addressed through gain-of-function studies.

284   Compared to previous genetic screens focused primarily on toxicity, our work identifies
285   cellular mechanisms upstream of protein aggregation. Despite our ability to identity components
286   of the endolysosomal pathway responsible for trafficking, the use of Lipofectamine may prevent
287   our detection of some very early cellular components important for α-synuclein uptake, such as
288   the receptor Lag3[36] and other early endocytic factors. Future screens in iPSC-derived neurons
289   using our newly developed platform[23] may uncover additional mechanisms critical to both α-
290   synuclein aggregation and toxicity in specific neuronal subtypes.

291

292   **MATERIALS AND METHODS**

293

294   **Purification, fibrillization, characterization and labelling of recombinant α-synuclein**

295

296   Human WT, A53T and E46K α-synuclein proteins were expressed in BL2-Gold(DE3)
297   competent cells (Agilent, Cat #230132). Protein expression was induced at log phase with 200
298   μM IPTG for 16 hours at room temperature. Cells were lysed in TE buffer (1 mM EDTA in 10
299   mM Tris pH 8.0 containing protease inhibitors) using sonication and the suspension was boiled
300   for 30 min. The lysate was clarified and α-synuclein was subsequently precipitated with
301   ammonium sulfate (361 mg/mL). The resulting pellet was resuspended in 50 ml of 25 mM
302   sodium phosphate buffer and run over a HiTrapQ-HP 5 mL column (Cytiva, Cat# 17115401). α-
303   synuclein was eluted with elution buffer (25 mM sodium phosphate buffer with 1 M NaCl over a
304   gradient). Fractions containing α-synuclein confirmed by Coomassie-stained SDS-PAGE were
305   dialyzed into PBS and concentrated with an Amicon Ultra-15 centrifugal 3 kDa MWCO filter
306   (Millipore, Cat# UFC900324), filter sterilized with using a Millex-GV syringe filter unit
307   (Millipore, Cat# SLGV033RB), and snap frozen in PBS at -80°C.

308   Aggregation was induced by agitating 5 mg/mL α-synuclein at 37 °C for 7 days 1200
309   rpm (VWR, Cat#12620-942). Fibril formation was evaluated by electron microscopy (see next
310   section for details). Resulting fibrils were diluted in PBS to 0.25 mg/mL transferred to sonication
311   tubes (Diagenode Cat# C30010011) and sonicated (Diagenode Bioruptor Pico, Cat# B01060010)
312   to generate fibril seeds for cell-based assays.

313   In order to monitor the kinetics of α-synuclein fibril formation *in vitro* 20 μM of
314   Thioflavin T was incubated with 5 mg/mL WT, A53T, or E46K monomer for 3 days at 37 °C
315   with continuous shaking and monitored via Thioflavin T fluorescence (excitation=444 nm,

7

316   emission=485 nm, cutoff=480 nm) in a Spectramax M5 microplate reader (Molecular Devices).
317   Readings were taken every 15 min.
318   To generate fluorescently labeled fibrils, 0.6 µl of 10 mg/ml of Alexa Fluor 555
319   (ThermoFisher, Cat# A37571), 100 µl of 0.25 mg/ml of fibrils, and 9.4 µl of 1 M sodium
320   bicarbonate were mixed at room temperature in the dark for 1 hour. Labeled α-synuclein fibrils
321   were separated from unlabeled dye with using a Zebra 7k MWCO spin desalting column
322   (ThermoFisher, Cat# 89882).
323
324   **Preparation of fibrils from multiple system atrophy patient brains**
325
326   Phosphotungstic acid (PTA) was performed as described ([6,37,38]). Briefly, 10% (w/v)
327   brain homogenate was incubated in 2% (v/v) sarkosyl (Sigma, 61747-100ML) and 0.5% (v/v)
328   benzonase (Sigma, # E104-25KU) at 37 °C with constant agitation (1,200 rpm) in an orbital
329   shaker for 2 hours. 10% Sodium PTA (Sigma, P6395-100G) was dissolved in water, and the pH
330   was adjusted to exactly 7.0. The 10% NaPTA solution was added to the solution to a final
331   concentration of 2% (v/v), which was agitated (1,200 rpm) in an orbital shaker overnight. The
332   sample was centrifuged at $16,000 \times g$ for 30 min at room temperature, and the supernatant was
333   carefully removed. The pellet was resuspended in 2% (v/v) sarkosyl in DPBS and 2% (v/v) PTA
334   in water, pH 7.0. The sample was again incubated for at least 1 hour before a second
335   centrifugation. The supernatant was removed, and the pellet was resuspended in DPBS using
336   10% of the initial starting volume. This suspension was diluted 1:20 in DPBS before use in cell-
337   based assays.
338
339   **Electron microscopy**
340
341   α-synuclein fibrils were negatively stained with 0.75% uranyl formate (pH 5.5–6.0) on
342   thin amorphous carbon-layered 400-mesh copper grids (Pelco Cat# 1GC400). 5 µl of 5 mg/mL
343   fibrils was applied to the grid for 1 min before removing the droplet with Whatman paper,
344   followed by two washes with 5 µl of ddH$_2$O and two applications of 5 µl of uranyl formate
345   removed by vacuum. Grids were imaged at room temperature using a Fei Tecnai 12 microscope
346   operating at 120 kV. Images of WT and A53T fibrils were captured on a US 4000 CCD camera
347   at x44117 resulting in a sampling of 3.4 Å/pixel. E46K fibrils were imaged on the microscope at
348   x57692 resulting in a sampling of 2.6 Å/pixel.
349
350   **Plasmid and library design**
351
352   Plasmids for the FRET-aggregation reporters were generated by subcloning full length
353   human α-synuclein PCR-amplified from pCAGGS-aSyn-CFP (a gift from Robert Edwards and
354   Ken Nakamura)[39] to the C-terminal Clover2 or mRuby2 into the lentiviral expression vector
355   pMK1200 (Addgene #84219)[21] under the control of the constitutive EF1A promoter, to obtain
356   pSKS40 and pSKS41, respectively. Point mutations were generated using QuikChange II site-
357   directed mutagenesis kits (Agilent, Cat# 200521) according to the manufacturers protocols in
358   pSKS40 and pSKS41 to generate α-synuclein(A53T)-mClover2 (pSKS42), α-synuclein(E46K)-
359   mClover2 (pSKS44), α-synuclein(A53T)-mRuby2 (pSKS43), synuclein(A53T)-mRuby2
360   (pSKS45).

The α-synuclein(WT) bacterial expression plasmid was a gift from Stanley Prusiner. Point mutations were generated using QuikChange II site-directed mutagenesis kit to generate α-synuclein(A53T) (pSKS28) and α-synuclein(E46K) (pSKS39) plasmids for bacterial expression.

Pooled CRISPRi sgRNA libraries genome-wide libraries were previously designed and validated.[40]

For generation of individual sgRNAs for focused retest screens, pairs of oligonucleotides (IDT) were annealed and ligated into our lentiviral sgRNA expression vector.

For stable expression of the CRISPRi machinery, we established lentiviral dCas9 expression vectors.[41]

The autophagy reporter plasmid pRT48 (CAG-GFP-LC3-RFP-LC3ΔG) was generated by subcloning the GFP-LC3-RFP-LC3ΔG-IRES-PuroR cassette from pMRX-IP-GFP-LC3-RFP-LC3ΔG (a gift from Noboru Mizushima and Addgene plasmid # 84572) to a lentiviral backbone downstream of a CAG promoter.

Cell culture and cell line generation

HEK293T cells were cultured in DMEM supplemented with 10% fetal bovine serum (Seradigm Cat# 97068- 085, lot 076B16), Pen/Strep (Life Technologies, Cat# 15140122), and L-glutamine (Life Technologies, Cat# 25030081). All cells were grown in a tissue culture incubator (37 °C, 5% CO_2) and regularly tested for mycoplasma contamination.

To introduce CRISPRi functionality to HEK293T cells, pHR-SFFV-dCas9-BFP-KRAB (Addgene #46911),[20] a gift from Stanley Qi and Jonathan Weissman was stably expressed in HEK293T cells, and a monoclonal cell line (cSKS197) was selected and validated as previously described.[23]

To generate the three FRET reporter lines, cSKS197 cells were infected with lentivirus from plasmids pSKS40/pSKS41, pSKS42/pSKS43, pSKS44/pSKS45, and cells with the highest dynamic FRET signal 24 hours after seeding with fibrils were selected.

LAMP1 and EEA1 endolysosomal markers were endogenously labeled using the split-mNeonGreen2 system.[42] Briefly, synthetic guide RNAs (IDT) were first complexed *in vitro* with purified *Streptococcus pyogenes* Cas9 protein (UC Berkeley Macrolab). Cas9/RNA complexes were then mixed with ssDNA oligo donors (IDT) and nucleofected (Lonza Cat# AAF-1002B, Amaxa program CM-130) into HEK293T cells stably expressing SFFV-mNeonGreen21–10. Fluorescent cells were selected by flow cytometry. Sequences for CRISPR RNA and donors used are listed as follows: LAMP1 (C-term mNG11): crRNA sequence, 5'-GTGCACCAGGCTAGATAGTC-3'; donor oligonucleotide sequence, 5'-CCCAGAGAAAGGAACAGAGGCCCCTGCAGCTGCTGTGCCTGCGTGCACCAGGCTAC ATCATATCGGTAAAGGCCTTTTGCCACTCCTTGAAGTTGAGCTCGGTACCACTTCCTG GACCTTGAAACAAAACTTCCAATCCGCCACCGATAGTCTGGTAGCCTGCGTGACTCC TCTTCCTGCCGACGAGGTAGGCGATGAGG-3'; EEA1 (N-term mNG11): crRNA sequence, 5'-GTGGTGGTTAAACCATGTTA-3'; donor oligonucleotide sequence, 5'-CCCGCGCAGGGTCTGGAGAGTCACCGCGGCGGCGCCGGGTGGTGGTTAAACCATGA CCGAGCTCAACTTCAAGGAGTGGCAAAAGGCCTTTACCGATATGATGGGTGGCGGA TTGGAAGTTTTGTTTCAAGGTCCAGGAAGTGGTTTAAGGAGGATTTTACAGAGGGTA AGAGAGTGAAACCGTCTTTCTGGCAGCACGT-3'

405   To generate CRISPRi- HEK293T cells that monitor endolysosomal damage , CRISPRi-
406 HEK293T cells were transduced with the fluorescent Gal3 reporter (pJC41),[41] and a polyclonal
407 population was sorted by FACS.
408   The GFP-LC3-RFP-LC3ΔG reporter line was generated as follows: HEK293T cells
409 stably expressing dCas9-BFP-KRAB was transduced with pRT48 and a monoclonal line was
410 selected for a high dynamic range for autophagic flux and high CRISPRi activity.
411
412 **Primary CRISPRi genome-wide screen**
413
414   The genome-wide screen was carried out as seven parallel screens with sublibraries H1-
415 H7.[40] For each sublibrary, 100 million HEK293T cells were seeded into a 15 cm^2 plate with
416 complete DMEM and transfected with 5 µg of lentiviral plasmid packaging mix and 5 µg of
417 pooled sgRNA library plasmid using lipofectamine 2000 (ThermoFisher Cat# 11668019) and
418 incubated for 2 days.
419   Lentivirus-containing media was removed and filter sterilized using a Millex-GV syringe
420 filter unit (Millipore Cat# SLGV033RB). For each library, 80 million FRET reporter cells were
421 infected with filtered lentivirus-containing media for a target MOI of ~30-70%. Infected cells
422 were selected with puromycin (1 ng/µL) for three days until % BFP >95%. Puromycin selected
423 cells were then seeded at 25,000 cells/ well into fifty 96-well plates (ThermoFisher Cat#
424 12556008) with 0.25 ug/mL fibrils and 0.002% (v/v) lipofectamine. After 24 hours, cells were
425 removed from the plates and sorted into FRET negative and FRET positive populations.
426 Genomic DNA was isolated using the Macherey-Nagel Blood L kit (Machery-Nagel Cat#
427 740954.20) according to the manufacturer's protocol. SgRNA-encoding cassettes were then
428 amplified by PCR, purified using SPRI-select beads, and deep-sequenced as previously
429 published.[23] Phenotypes and P values for each gene were generated using the following pipeline:
430 (https://kampmannlab.ucsf.edu/mageck-inc).[23]
431
432 **Microscopy and Flow cytometry secondary assays**
433
434   To monitor α-synuclein aggregation, FRET reporter cells were seeded (25,000 cells/well)
435 into 70 µL per well in a 96 well plates. In each well, 3 µL 0.25 mg/mL fibrils were complexed
436 with 0.2 µL Lipofectamine 2000 for 1 hour at room temperature and added to 27 µL Optimem
437 (ThermoFisher Cat# 31985070). The complex in Optimem was then added to pre-seeded reporter
438 cells in 96-well plates and analyzed 24 hours after seeding. For analysis, cells were stained with
439 Hoechst 33342 (ThermoFisher Cat# 5553141) at 0.5 µg/mL and analyzed by flow cytometry
440 using a BD FACSCelesta or by fluorescence microscopy using an InCell 6000 (GE Cat# 28-
441 9938-51). Cells with sgRNA knockdown were similarly analyzed using a comparable protocol 5
442 days after transduction with individual sgRNA-encoding lentivirus.
443   To monitor fibril uptake, CRISPRi-HEK293T cells were seeded (25,000 cells/well) into
444 70 µL in a 96-well plate with 3 µL of 0.25 mg/mL fibrils complexed with 0.2 µL Lipofectamine
445 2000 in 30 µL of Optimem, with various apilimod concentrations. Cells collected were collected
446 at various timepoints until t = 6 hours after seeding for analysis by flow cytometry. Median
447 mClover2 values were calculated in FlowJo and averaged between 3 technical replicates.
448   To monitor plasmid uptake, CRISPRi-HEK293T cells were seeded into 24-well plates at
449 200,000 cells/well and cultured for 24 hours. 5 ng of Plg15-BFP[18] DNA complexed with 3 µL of
450 Lipofetamine in 100 µL Optimem and various concentrations of apilimod was added to each

10

451 well. After 24 hours cells were collected and analyzed via flow cytometry. Median BFP values
452 were calculated in FlowJo and averaged between 2 technical replicates.
453   To monitor α-synuclein-Clover2 steady-state levels, FRET reporter was treated with
454 various apilimod concentrations were seeded (25,000 cells/well) into 70 µL in a 96-well plate
455 with 3 µL of 0.25 mg/mL fibrils was complexed with 0.2 µL Lipofectamine 2000 in 30 µL of
456 Optimem. Median Clover2 values were calculated in FlowJo and averaged between 3 technical
457 replicates.
458   To monitor autophagy, the CRISPRi-HEK293T cells expressing GFP-LC3-RFP-LC3ΔG
459 reporter were seeded (25,000 cells/well) into 70 µL in a 96-well plate with 3 µL of 0.25 mg/mL
460 fibrils complexed with 0.2 µL Lipofectamine 2000 in 30 µL of Optimem, with various apilimod,
461 bafilomycin and torin concentrations. After 24 hours cells were collected and analyzed via flow
462 cytometry. The ratio of RFP/GFP was calculated in FlowJo and averaged between 3 technical
463 replicates.
464   To monitor Gal3-EGFP puncta formation, CRISPRi-HEK293T cells expressing EGFP-
465 Gal3 were seeded (25,000 cells/well) into 70 µL/ well in a 96-well black bottom plates, exposed
466 to 3 µL of 0.25 mg/mL fibrils was complexed with 0.2 µL Lipofectamine 2000 in 30 µL of
467 Optimem, and treated with LLOME or Lipofectamine at varying concentrations. 24 hours after
468 seeding, cells were stained with Draq5 (Abcam, Cat# 108410) and images were collected by an
469 InCell 6000. Images were analyzed using CellProfiler by quantifying the integrated density of
470 identified Gal3 puncta divided by Draq5-stained nuclei and averaged between 3 images.
471   To track fibrils through the endolysosomal system in cells, LAMP1 and EEA1 were first
472 pre-stained HEK293T cells with Hoechst diluted 1:10,000 in DMEM for 30 minutes at 37 °C,
473 and first seeded (28,000 cells/well) into 150 µL microscopy media (DMEM, 10% FBS, 1% L-
474 glutamine, 1% penicillin streptomycin, no phenol red) in a glass-bottom 96 well microscopy
475 plate (Grenier, Cat# 655891) coated with fibronectin. The cells were then allowed to rest for half
476 an hour at 37 °C. At the half hour mark, the cells were treated with either 360 nM apilimod or
477 DMSO. The plate was then transferred to the microscope, and the pre-fibril images were
478 acquired. Forty minutes after drug treatment, 30 uL of the fibril mixture (4 µL of 0.25 mg/mL
479 Alexa 555-tagged fibrils complexed with 0.2 µL Lipofectamine 2000 in 28 µL of Optimem) was
480 added to the cells. Z-stacks were then taken 30 minutes, 1 hour, 2 hours, 4 hours and 24 hours
481 after the addition of fibrils using an Andor Dragonfly High Speed Confocal Platform. All images
482 were acquired at 63x magnification.
483
484 **Filter-trap and immunoblot**
485
486   FRET reporter cells were seeded (25,000 cells/well) in 70 µL per well into 96 well plates
487 with various concentrations of apilimod. In each well 3 µL 0.25 mg/mL α-synuclein fibrils was
488 complexed with 0.2 µL Lipofectamine 2000 for 1 hr at room temperature and added to 27 µL
489 Optimem (ThermoFisher Cat# 31985070). Cells were collected by centrifugation at 1000 x *g* for
490 5 min and washed twice with PBS. Pellets were resuspended in 100 µL RIPA buffer containing
491 protease inhibitors and homogenized on a tip sonicator (Sonopuls 2070) for 1 s at a power level
492 of 10% for 5 s. 50 µL of sample was removed added to 50 µL 1x TBS or 1x TBS + 8M Urea
493 mixed well. A dot blot vacuum manifold (Schleicher and Schuell Dot-Blot System) was used to
494 pull 50 µl of each sample through onto a 0.45 µm nitrocellulose membrane (Biorad, Cat#162-
495 0115). The membrane was washed 1x with water, blocked with Intercept Blocking Buffer
496 (LiCor, Cat# 927-70001). Primary antibodies against human α-synuclein (Thermo Fisher, Cat#

11

497 AHB0261) and GFP (Genetex, Cat# GTX113617) were used to detect proteins. Blots were then
498 incubated with secondary antibodies (LiCor catalog numbers 926-32213 and 926-68072) and
499 imaged on the Odyssey Fc Imaging system (LiCor, Cat# 2800). Immunoblot intensity was
500 normalized to protein concentration as determined by a BCA Protein Assay Kit (Pierce, Cat#
501 23225). Images were processed and analyzed using LiCor Image Studio^{TM} software.
502
503 **qRT-PCR**
504
505   CRISPRi-HEK293T cells expressing a nontargeting or targeting sgRNA were collected
506 by centrifugation at 1000 x g for 5 min and washed twice with PBS. RNA was purified using a
507 RNA purification kit (Zymo, Cat#R1051). 500 ng of total RNA from each sample were reverse
508 transcribed to cDNA using the Bioline SensiFAST cDNA Synthesis kit (Bioline, Cat# BIO-
509 65054). The cDNA was diluted 13-fold in ddH2O and 4 uL of this dilution was used for each
510 quantitative real-time PCR (qPCR). qPCR reactions were set up using SensiFast 2x Mastermix
511 (Bioline Cat# BIO-94020) and oligonucleotides targeting genes of interest (IDT) in triplicate and
512 run on the Quantstudio6 according to manufacturer's protocols. Reactions were normalized to
513 *GAPDH* as an internal loading control. sgRNA activity is expressed as knockdown efficiency.
514 qPCR results and primer sequences are provided in Table S2.
515
516
517 **AUTHOR CONTRIBUTIONS**:
518 S.K.S. and M.K. conceptualization; S.K.S., M.C., S.B., R.T., A.W., E.T., I.E.J., C.N. E.N.M.,
519 J.S., M.D.L. and M.K. resources; S.K.S and M.K. formal analysis; S.K.S., M.C., S.B., R.T.,
520 A.W., E.T., I.E.J., C.N. E.N.M., J.S., M.D.L. and M.K. investigation; S.K.S and M.K.
521 methodology; S.K.S and M.K. writing-original draft; S.K.S., M.C., S.B., R.T., A.W., E.T., I.E.J.,
522 C.N. E.N.M., J.S., D.R.S., J.E.S., M.D.L. and M.K. writing review and editing; R.T. and M.K.
523 software; D.R.S., J.E.G., and M.K. funding acquisition; M.K. supervision.
524
525
526 **ACKNOWLEDGEMENTS:**
527 We thank Ana Maria Cuervo, Robert Edwards, Matt Jacobson, Carmen Nussbaum, Xiaoyan
528 Guo, Nina Dräger, Emmy Li, Kun Leng, and other members of the Kampmann Lab for helpful
529 discussions on experimental design and interpretation. We thank all co-authors, Avi Samelson,
530 and Xiaoyan Guo for discussions and feedback on the manuscript. We thank Eric Chow and
531 Derek Bogdanoff (UCSF Center for Advanced Technology) for support with next-generation
532 sequencing and Sarah Elmes (UCSF Laboratory for Cell Analysis) for support with FACS. This
533 work was supported by a Department of Defense NDSEG fellowship (S.K.S.), NIH grants DP2
534 GM119139 and R01 AG062359 (M.K.).
535
536
537 **COMPETING INTERESTS**:
538 None.
539

REFERENCES

1. Prusiner, S. B. Novel proteinaceous infectious particles cause scrapie. *Science (80-.).* (1982) doi:10.1126/science.6801762.

2. Jucker, M. & Walker, L. C. Self-propagation of pathogenic protein aggregates in neurodegenerative diseases. *Nature* (2013) doi:10.1038/nature12481.

3. Brettschneider, J., Del Tredici, K., Lee, V. M. Y. & Trojanowski, J. Q. Spreading of pathology in neurodegenerative diseases: A focus on human studies. *Nature Reviews Neuroscience* (2015) doi:10.1038/nrn3887.

4. Prusiner, S. B. Biology and genetics of prions causing neurodegeneration. *Annual Review of Genetics* (2013) doi:10.1146/annurev-genet-110711-155524.

5. Goedert, M. Alpha-synuclein and neurodegenerative diseases. *Nature Reviews Neuroscience* (2001) doi:10.1038/35081564.

6. Woerman, A. L. *et al.* Propagation of prions causing synucleinopathies in cultured cells. *Proc. Natl. Acad. Sci. U. S. A.* (2015) doi:10.1073/pnas.1513426112.

7. Luk, K. C. *et al.* Exogenous α-synuclein fibrils seed the formation of Lewy body-like intracellular inclusions in cultured cells. *Proc. Natl. Acad. Sci. U. S. A.* (2009) doi:10.1073/pnas.0908005106.

8. Holmes, B. B. *et al.* Proteopathic tau seeding predicts tauopathy in vivo. *Proc. Natl. Acad. Sci. U. S. A.* (2014) doi:10.1073/pnas.1411649111.

9. Yamasaki, T. R. *et al.* Parkinson's disease and multiple system atrophy have distinct -synuclein seed characteristics. *J. Biol. Chem.* (2019) doi:10.1074/jbc.RA118.004471.

10. Prusiner, S. B. *et al.* Evidence for α-synuclein prions causing multiple system atrophy in humans with parkinsonism. *Proc. Natl. Acad. Sci. U. S. A.* (2015) doi:10.1073/pnas.1514475112.

11. Woerman, A. L. *et al.* Familial Parkinson's point mutation abolishes multiple system atrophy prion replication. *Proc. Natl. Acad. Sci. U. S. A.* (2017) doi:10.1073/pnas.1719369115.

12. Delenclos, M. *et al.* Cellular models of alpha-synuclein toxicity and aggregation. *Journal of Neurochemistry* (2019) doi:10.1111/jnc.14806.

13. Höllerhage, M., Bickle, M. & Höglinger, G. U. Unbiased Screens for Modifiers of Alpha-Synuclein Toxicity. *Current Neurology and Neuroscience Reports* (2019) doi:10.1007/s11910-019-0925-z.

14. Khurana, V. *et al.* Genome-Scale Networks Link Neurodegenerative Disease Genes to α-Synuclein through Specific Molecular Pathways. *Cell Syst.* (2017) doi:10.1016/j.cels.2016.12.011.

15. Rousseaux, M. W. C. *et al.* TRIM28 regulates the nuclear accumulation and toxicity of both alpha-synuclein and tau. *Elife* (2016) doi:10.7554/eLife.19809.

16. Rousseaux, M. W. C. *et al.* A druggable genome screen identifies modifiers of α-synuclein levels via a tiered cross-species validation approach. *J. Neurosci.* (2018) doi:10.1523/JNEUROSCI.0254-18.2018.

17. Vázquez-Vélez, G. E. *et al.* Doublecortin-like Kinase 1 Regulates α-Synuclein Levels and Toxicity. *J. Neurosci.* (2020) doi:10.1523/JNEUROSCI.1076-19.2019.

18. Gilbert, L. A. *et al.* Genome-Scale CRISPR-Mediated Control of Gene Repression and Activation. *Cell* (2014) doi:10.1016/j.cell.2014.09.029.

19. Kampmann, M. CRISPRi and CRISPRa Screens in Mammalian Cells for Precision

586   Biology and Medicine. *ACS Chem. Biol.* (2018) doi:10.1021/acschembio.7b00657.

587   20.   Gilbert Luke A *et al.* CRISPR-mediated modular RNA-guided regulation of transcription
588   in eukaryotes. *Cell* (2013).

589   21.   Kampmann, M., Bassik, M. C. & Weissman, J. S. Integrated platform for genome-wide
590   screening and construction of high-density genetic interaction maps in mammalian cells.
591   *Proc. Natl. Acad. Sci. U. S. A.* (2013) doi:10.1073/pnas.1307002110.

592   22.   Kampmann, M., Bassik, M. C. & Weissman, J. S. Functional genomics platform for
593   pooled screening and generation of mammalian genetic interaction maps. *Nat. Protoc.*
594   (2014) doi:10.1038/nprot.2014.103.

595   23.   Tian, R. *et al.* CRISPR Interference-Based Platform for Multimodal Genetic Screens in
596   Human iPSC-Derived Neurons. *Neuron* (2019) doi:10.1016/j.neuron.2019.07.014.

597   24.   Sbrissa, D., Ikonomov, O. C. & Shisheva, A. PIKfyve, a mammalian ortholog of yeast
598   Fab1p lipid kinase, synthesizes 5-phosphoinositides. Effect of insulin. *J. Biol. Chem.*
599   (1999) doi:10.1074/jbc.274.31.21589.

600   25.   Webb, J. L., Ravikumar, B., Atkins, J., Skepper, J. N. & Rubinsztein, D. C. α-synuclein Is
601   Degraded by Both Autophagy and the Proteasome. *J. Biol. Chem.* (2003)
602   doi:10.1074/jbc.M300227200.

603   26.   Kaizuka, T. *et al.* An Autophagic Flux Probe that Releases an Internal Control. *Mol. Cell*
604   (2016) doi:10.1016/j.molcel.2016.09.037.

605   27.   Lee, H. J. *et al.* Autophagic failure promotes the exocytosis and intercellular transfer of α-
606   synuclein. *Exp. Mol. Med.* (2013) doi:10.1038/emm.2013.45.

607   28.   de Lartigue, J. *et al.* PIKfyve regulation of endosome-linked pathways. *Traffic* (2009)
608   doi:10.1111/j.1600-0854.2009.00915.x.

609   29.   Jiang, P., Gan, M., Yen, S. H., McLean, P. J. & Dickson, D. W. Impaired endo-lysosomal
610   membrane integrity accelerates the seeding progression of α-synuclein aggregates. *Sci.*
611   *Rep.* (2017) doi:10.1038/s41598-017-08149-w.

612   30.   Aits, S. *et al.* Sensitive detection of lysosomal membrane permeabilization by lysosomal
613   galectin puncta assay. *Autophagy* (2015) doi:10.1080/15548627.2015.1063871.

614   31.   Thiele, D. L. & Lipsky, P. E. Mechanism of L-leucyl-L-leucine methyl ester-mediated
615   killing of cytotoxic lymphocytes: Dependence on a lysosomal thiol protease, dipeptidyl
616   peptidase I, that is enriched in these cells. *Proc. Natl. Acad. Sci. U. S. A.* (1990)
617   doi:10.1073/pnas.87.1.83.

618   32.   Staats, K. A. *et al.* Small molecule inhibition of PIKFYVE kinase rescues gain- and loss-
619   of-function C9ORF72 ALS/FTD disease processes in vivo. *bioRxiv* (2019)
620   doi:10.1101/685800.

621   33.   Kang, Y. *et al.* Inhibition of PIKfyve kinase prevents infection by Zaire ebolavirus and
622   SARS-CoV-2. *Proc. Natl. Acad. Sci. U. S. A.* (2020) 117(34): 20803-20813.

623   34.   Wentink, A. S. *et al.* Molecular dissection of amyloid disaggregation by human HSP70.
624   *Nature* (2020) doi:10.1038/s41586-020-2904-6.

625   35.   Muchowski, P. J. & Wacker, J. L. Modulation of neurodegeneration by molecular
626   chaperones. *Nature Reviews Neuroscience* (2005) doi:10.1038/nrn1587.

627   36.   Mao, X. *et al.* Pathological α-synuclein transmission initiated by binding lymphocyte-
628   activation gene 3. *Science (80-.).* (2016) doi:10.1126/science.aah3374.

629   37.   Safar, J. *et al.* Eight prion strains have PrP(Sc) molecules with different conformations.
630   *Nat. Med.* (1998) doi:10.1038/2654.

631   38.   Levine, D. J. *et al.* Mechanism of scrapie prion precipitation with phosphotungstate

632   anions. *ACS Chem. Biol.* (2015) doi:10.1021/cb5006239.
633 39. Fortin, D. L. *et al.* Lipid rafts mediate the synaptic localization of α-synuclein. *J.*
634   *Neurosci.* (2004) doi:10.1523/JNEUROSCI.1594-04.2004.
635 40. Horlbeck, M. A. *et al.* Compact and highly active next-generation libraries for CRISPR-
636   mediated gene repression and activation. *Elife* (2016) doi:10.7554/eLife.19760.
637 41. Chen, J. J. *et al.* Compromised function of the ESCRT pathway promotes endolysosomal
638   escape of tau seeds and propagation of tau aggregation. *J. Biol. Chem.* (2019)
639   doi:10.1074/jbc.RA119.009432.
640 42. Feng, S. *et al.* Improved split fluorescent proteins for endogenous protein labeling. *Nat.*
641   *Commun.* (2017) doi:10.1038/s41467-017-00494-8.
642
643
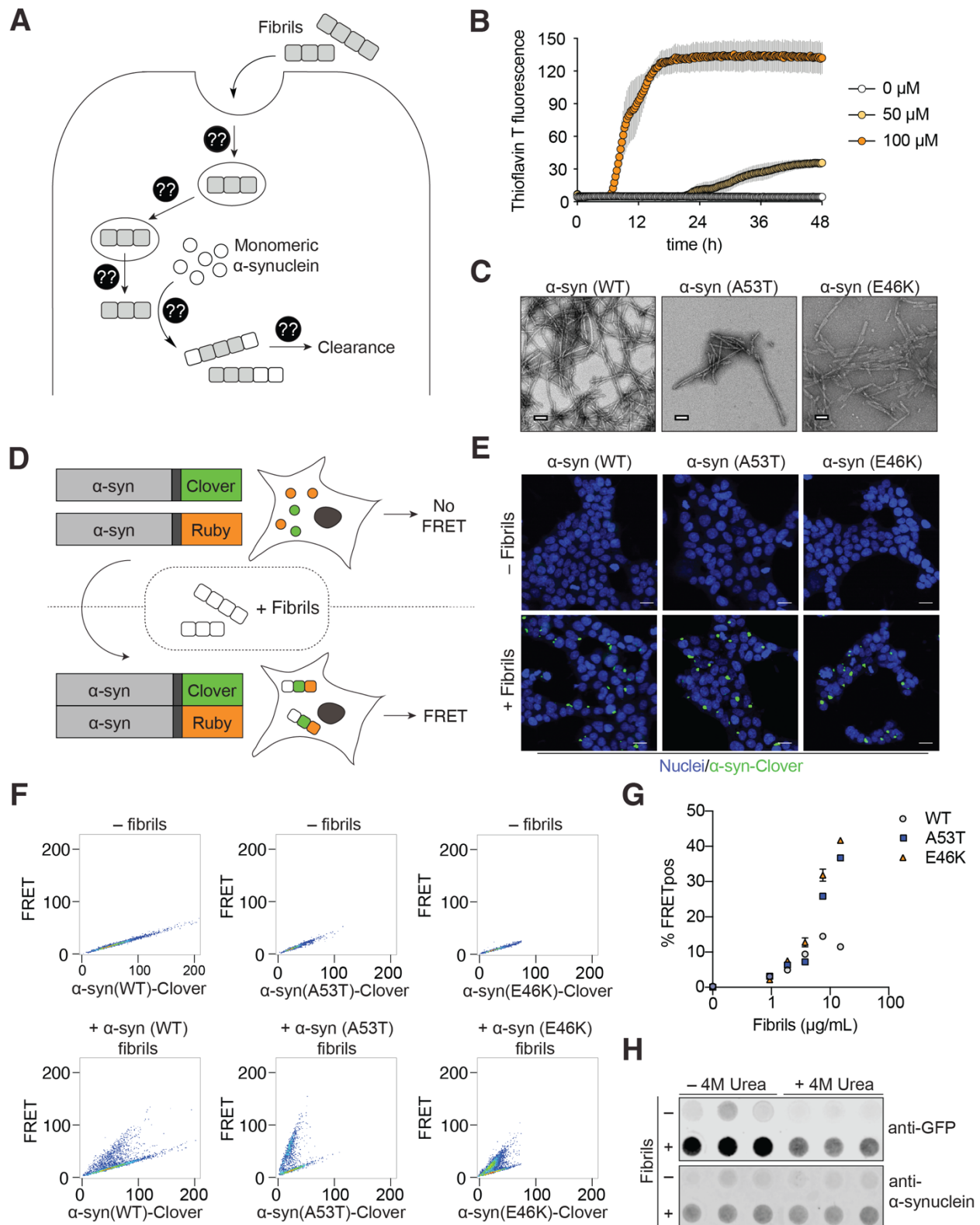
644
645
Fig. 1. A cell-based model of prion-like spreading α-synuclein aggregation. (A) Diagram of cellular
mechanisms that may control the prion-like spread of α-synuclein aggregation. Question marks represent
unknown cellular mechanisms and potential therapeutic targets. (B) Vigorous agitation of recombinant α-

16

649   synuclein monomers at 37°C induces fibrilization. Fibrilization is monitored by Thioflavin T fluorescence
650   (excitation: 440 nm, emission: 485 nm). Error bars represent mean ± S.E.M from n = 4 technical
651   replicates. (C) Representative negative stain electron micrographs α-synuclein fibrils formed from
652   recombinant protein with the WT sequence or the Parkinson's Disease-associated mutations A53T or
653   E46K. Scale bar: 100 nm. (D) Schematic of the FRET-based reporter system used to monitor α-synuclein
654   aggregation in HEK293T cells. In the absence of fibrils α-synuclein-Clover and α-synuclein-Ruby are
655   monomeric. Exposure to α-synuclein fibrils induces aggregation of the reporter. During aggregation, the
656   proximity of the fluorescently tagged α-synuclein can be detected by fluorescence microscopy or by flow
657   cytometry. (E) Representative fluorescence microscopy images of reporter cells exposed to α-synuclein
658   fibrils or lipofectamine alone. Blue: Draq5(nuclei). Green: α-synuclein-clover. Scale bar: 20 μm. (F)
659   Representative flow cytometry plots of the WT, A53T and E46K FRET reporter cells after 24 h treatment
660   with lipofectamine only (top row) or with α-synuclein fibrils (bottom row). (G) Quantification of %
661   FRET-positive cells using flow cytometry across concentration ranges of α-synuclein fibrils. Error bars
662   represent mean ± S.E.M from n = 3 technical replicates. (H) E46K FRET-reporter cells exposed to E46K
663   fibrils were passed through a 0.45 μm nitrocellulose membrane after lysis and 10 min incubation in either
664   TBS or 4M Urea. Insoluble material trapped on the membrane was quantified by immunoblotting against
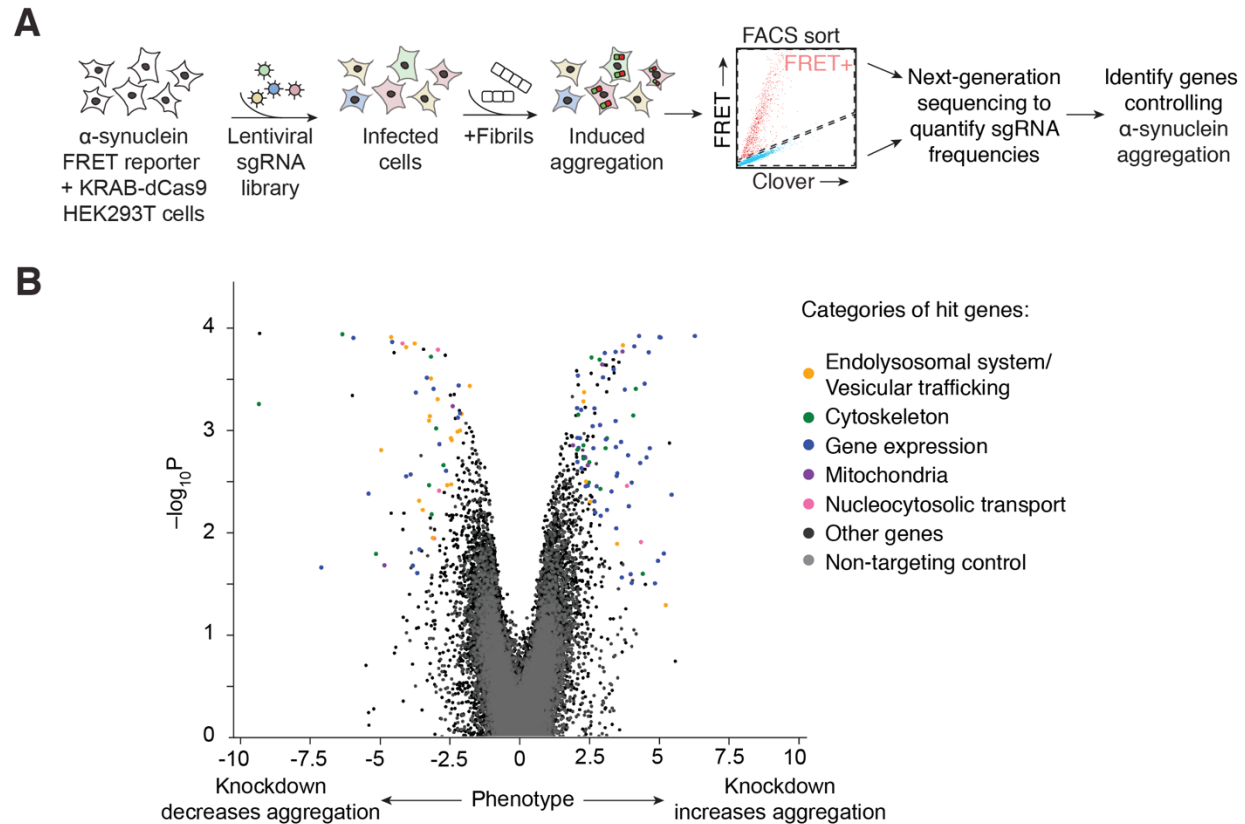665   the clover tag to detect intracellular α-synuclein.
666

Fig. 2. A genome-wide CRISPRi screen for cellular factors controlling α-synuclein aggregation.
(A) Schematic for a pooled FRET-based CRISPRi screen. FRET reporter cells stably expressing CRISPRi machinery (dCas9-BFP-KRAB) were transduced with pooled lentiviral libraries encoding sgRNAs targeting every protein-coding gene in the genome. Infected cells were then selected, expanded and exposed to α-synuclein fibrils. 24 hours later, cells were sorted into FRET-negative and FRET-positive populations by FACS. sgRNA-encoding cassettes were amplified from the genomic DNA of each population and sgRNA frequencies were quantified by next generation sequencing in order to identify genes that control α-synuclein aggregation. (B) Volcano plot of genes showing categories of major hit genes from the primary genome-wide screen.
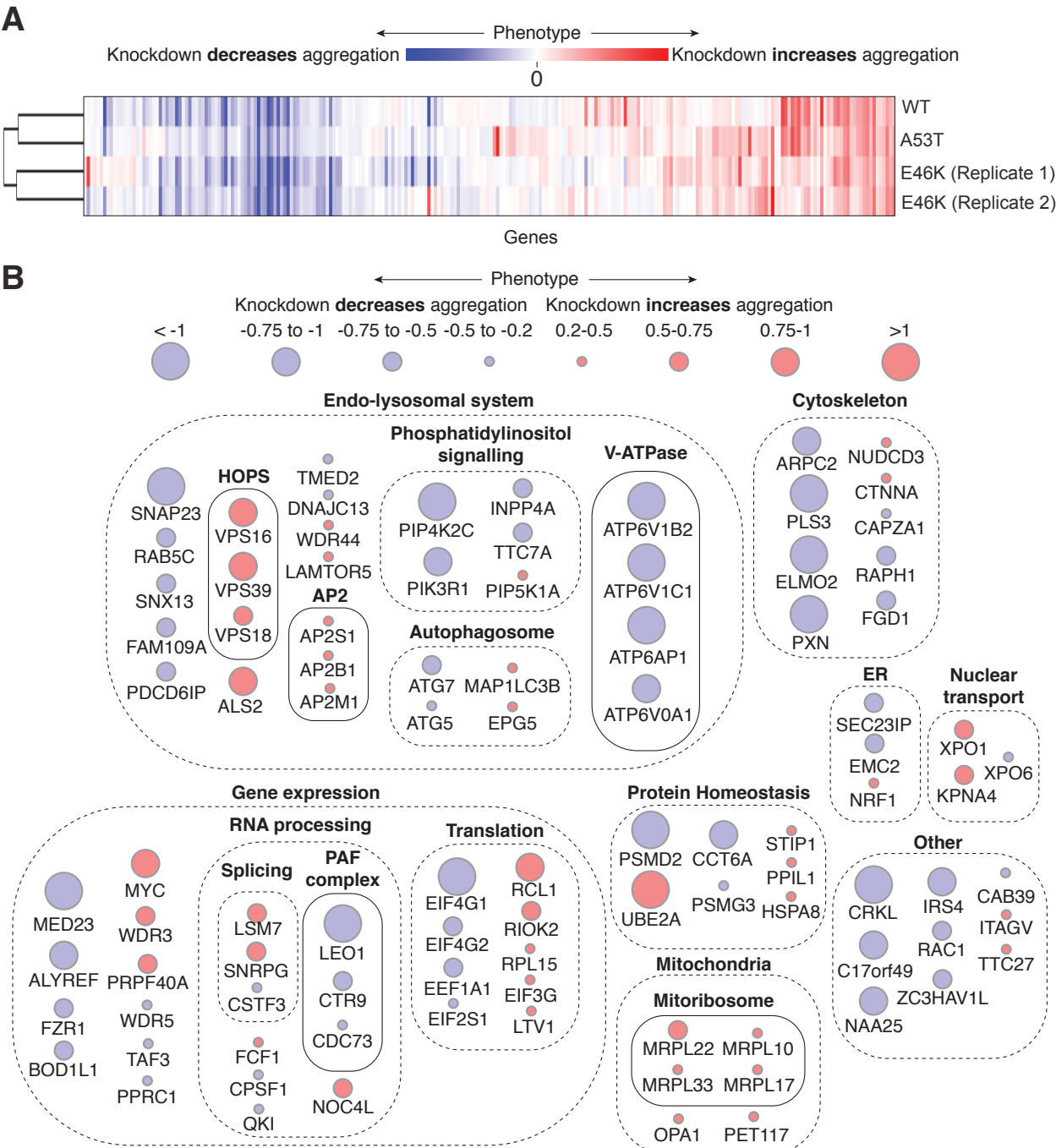
Fig. 3. Focused revalidation CRISPRi screen for cellular factors controlling α-synuclein aggregation. (A) Heat map summarizing the relative phenotypes from four focused secondary screens: WT, A53T and E46K reporters Genes selected for these focused screens were top representative hits from the primary genome-wide CRISPRi screen. (B) Overview of top hits from these focused screens, and the biological pathways in which they act.
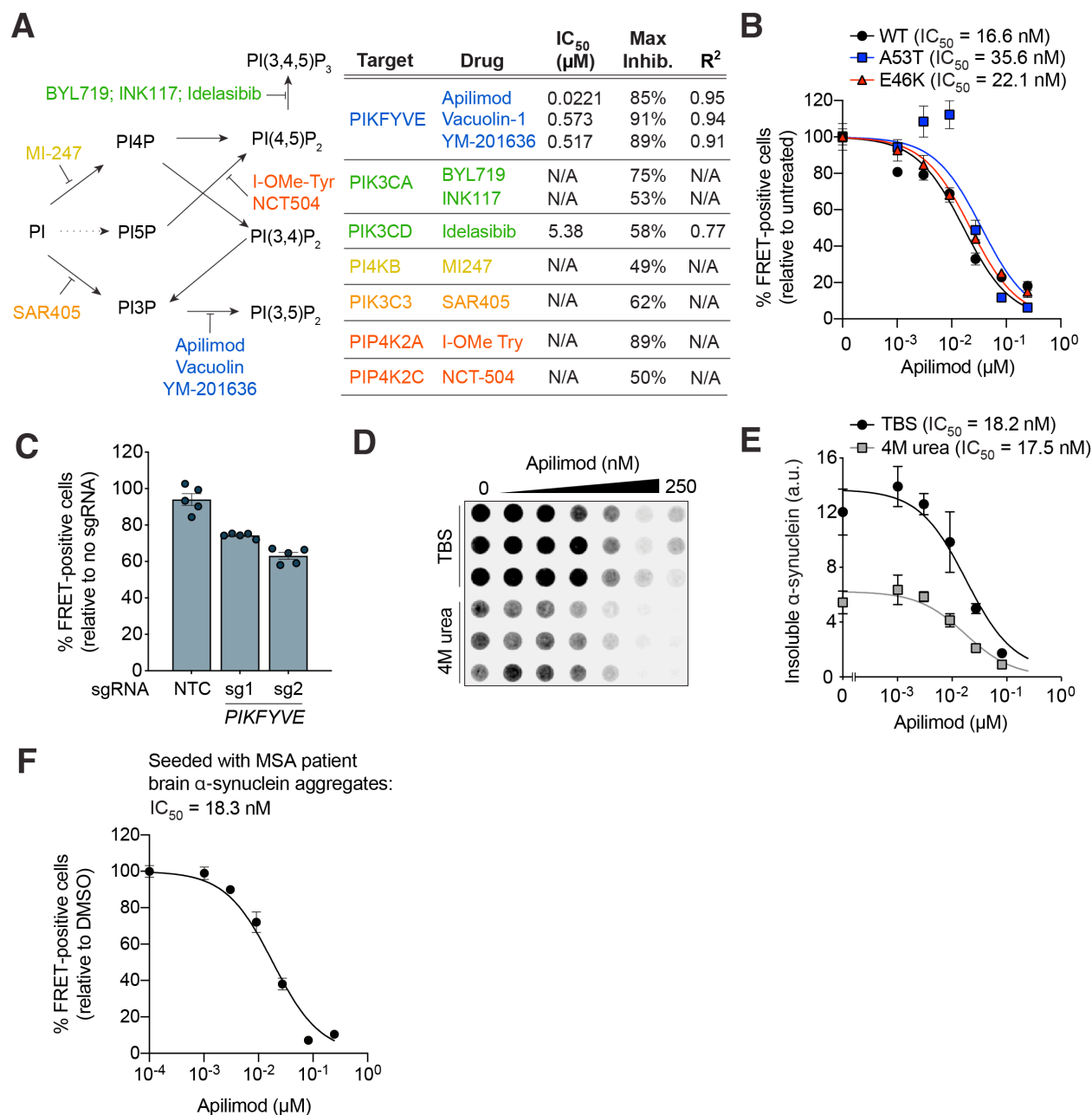
689

690
691
692
693 **Fig. 4. Inhibition of PIKFYVE decreases α-synuclein aggregation in FRET reporter cells seeded**
694 **with fibrils.** (A) Pharmacological inhibition of several kinases in the phosphatidylinositol pathway
695 decreases α-synuclein aggregation. FRET reporter cells were co-treated with fibrils and various
696 concentrations of each kinase inhibitor and collected for flow cytometry after 24 hours (also in
697 Supplemental Figure 1). (B) Dose-dependent decrease of aggregation in FRET reporter cells treated with
698 the PIKFYVE inhibitor apilimod. Error bars represent mean ± s.e.m from n = 3 technical replicates. (C)
699 FRET reporter cells were transduced with individual sgRNAs targeting PIKFYVE or a non-targeting
700 control sgRNA (NTC) and aggregation was measured 5 days after transduction. Error bars represent mean
701 ± S.E.M from n = 3 technical replicates. (D) Apilimod decreases insoluble intracellular α-synuclein.
702 FRET-reporter cells exposed to increasing apilimod concentrations were passed through a 0.45 μm

703   nitrocellulose membrane after lysis and 10 min incubation in either TBS or 4M Urea. Insoluble material
704   trapped on the membrane was quantified by immunoblotting against the clover tag to detect intracellular
705   α-synuclein. (E) Quantification of Fig. 3D. Immunoblot signal was normalized to lysate protein
706   concentration as determined by a BCA assay. Error bars represent mean ± S.E.M from n = 3 technical
707   replicates. (F) Dose-dependent decrease of aggregation trigged with MSA patient brain-derived fibrils
708   derived with the PIKFYVE inhibitor apilimod. Error bars represent mean ± s.e.m from n = 3 technical
709   replicates.
710
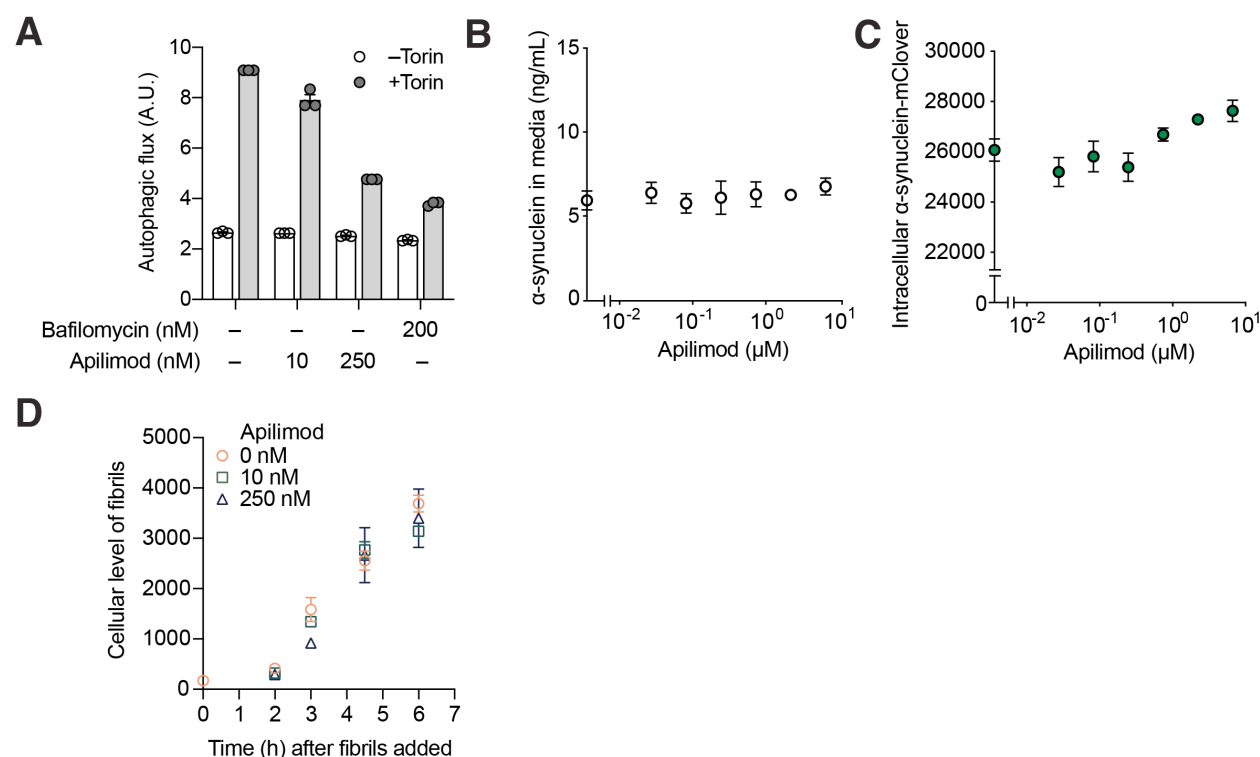
Fig 5. PIKFYVE inhibition decreases autophagic flux but does not affect α-synuclein export or fibril uptake. (A) CRISPRi-HEK293T cells expressing mCherry-GFP-LC3 were treated with either bafilomycin or apilimod in the presence and absence of torin. Changes in the ratio of GFP/mCherry was monitored by flow cytometry. Error bars represent mean ± S.E.M from n = 3 technical replicates. (B) α-synuclein and mClover protein detected in the media by ELISA. Error bars represent mean ± S.E.M from n = 3 technical replicates. (C) PIKFYVE inhibition does not impact steady-state levels of the α-synuclein-Clover2 construct in FRET reporter cells, as quantified by flow cytometry. Error bars represent mean ± S.E.M from n = 3 technical replicates. (D) PIKFYVE inhibition does not impact uptake of Alexa-555 tagged fibrils. Error bars represent mean ± S.E.M from n = 3 technical replicates.
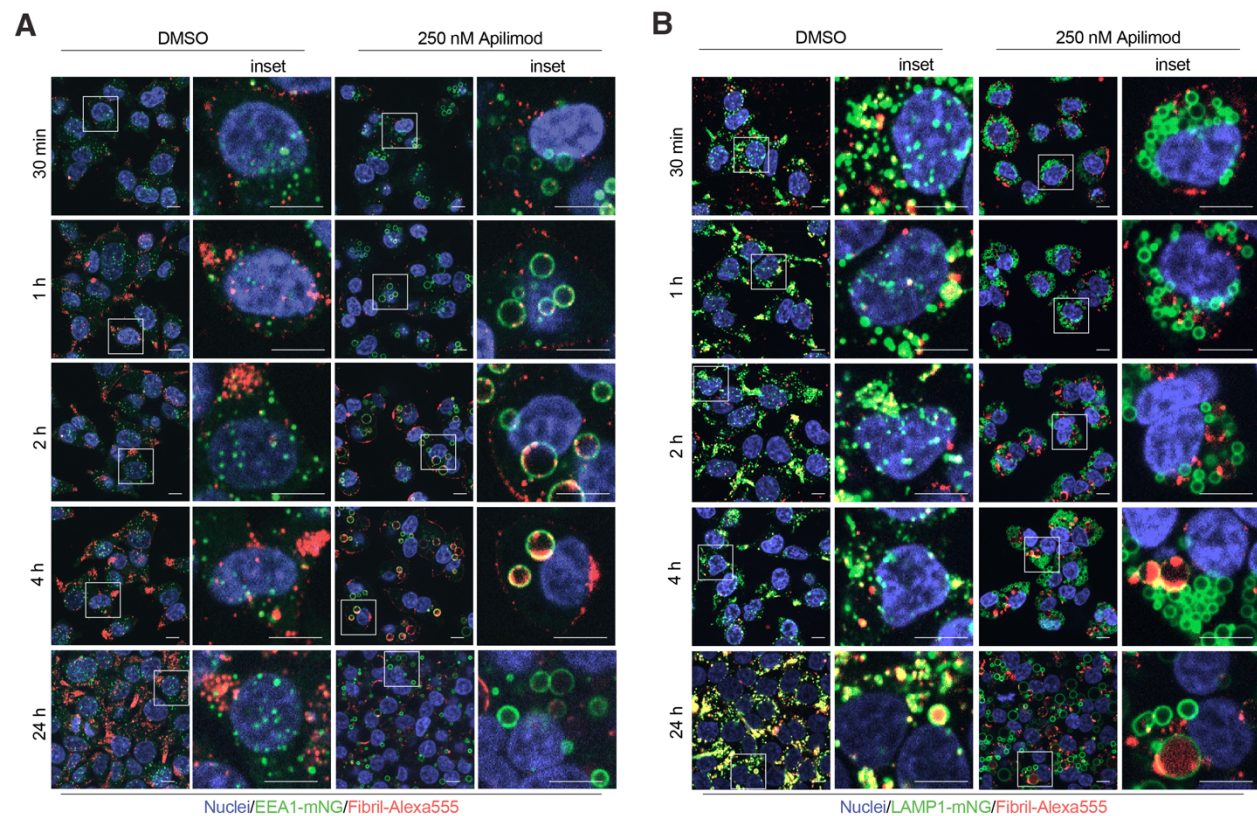
Nuclei/EEA1-mNG/Fibril-Alexa555

Nuclei/LAMP1-mNG/Fibril-Alexa555

Fig. 6. PIKFYVE inhibition interferes with α-synuclein fibril trafficking to the lysosome.
Representative fluorescence microscopy images of cells in which the early endosomal marker EEA1 (A) or the lysosomal marker LAMP1 (B) were endogenously labeled with the split-mNeonGreen system and exposed to fibrils tagged with Alexa555 in the presence and absence of Apilimod. Timepoints were acquired at 30 min, 1 h, 2h, 4h, and 24 h after fibril addition. Scale bar: 5 μm.

23
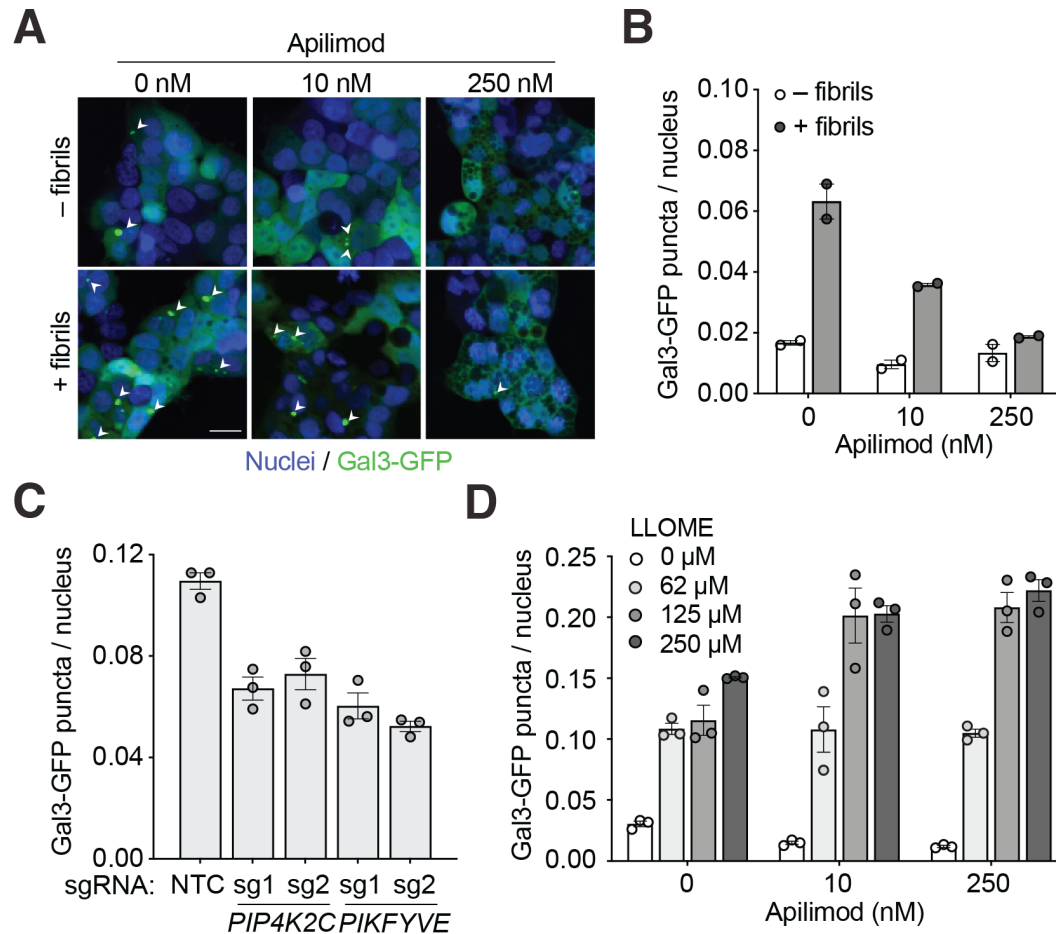
Fig. 7. PIKFYVE inhibition reduces fibril-induced lysosomal rupture. (A) Representative fluorescence microscopy images of CRISPRi-HEK293T cells expressing an EGFP-Galectin3 (EGFP-Gal3) reporter treated with apilimod. EGFP-Gal3 reporter cells were co-treated with fibrils and apilimod or DMSO 24 hours prior to imaging. Nuclei were counter-stained with Draq5. Scale bar: 20 μm. (B) Quantification of EGFP-Gal3 puncta divided by number of nuclei in fluorescence microscopy images shown in (A). Error bars represent mean ± S.E.M for $n = 2$ technical replicates (with at least 300 nuclei per image). (C) EGFP-Gal3 reporter cells were transduced with individual sgRNAs targeting PIP4K2C, PIKFYVE or a non-targeting control sgRNA (NTC). 5 days after transduction fibrils were added to EGFP-Gal3 reporter cells and puncta formation was observed by microscopy. Error bars represent mean ± S.E.M for $n = 3$ technical replicates (with at least 300 nuclei per image). (D) EGFP-Gal3 reporter cells were treated with various concentrations of LLOME and apilimod and 24 h after treatment puncta formation was observed by microscopy. Error bars represent mean ± S.E.M for $n = 3$ technical replicates (with at least 300 nuclei per image).
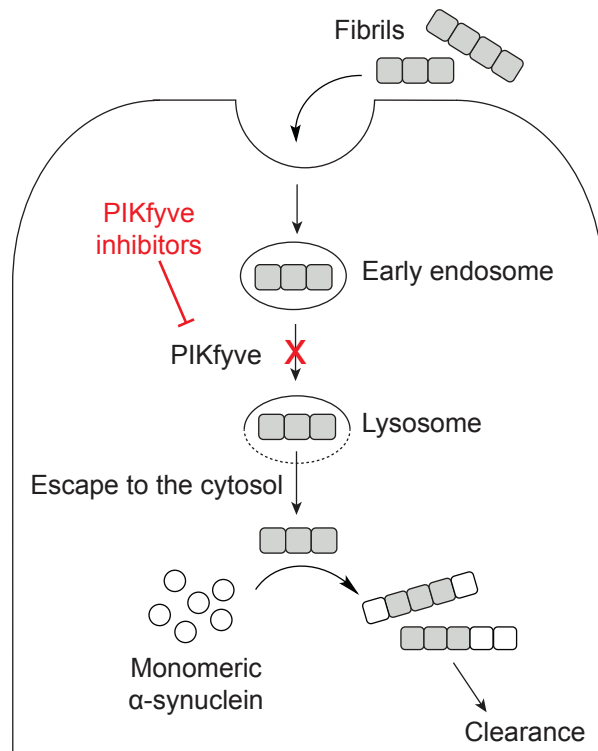
24

Fig. 8. Model. PIKfyve inhibition reduces propagation of α-synuclein aggregation in cells by limiting fibril access to the lysosome and lysosomal escape.
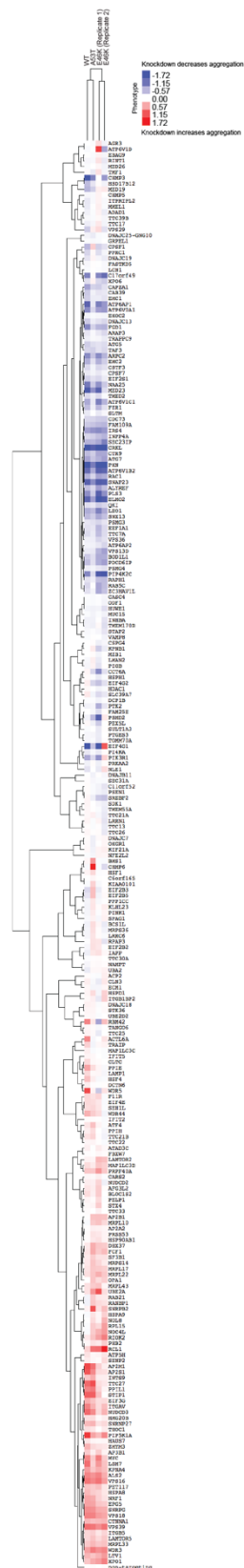
25

Fig. S1. Full heat map displaying gene names and clustering analysis shown in Fig. 3A.
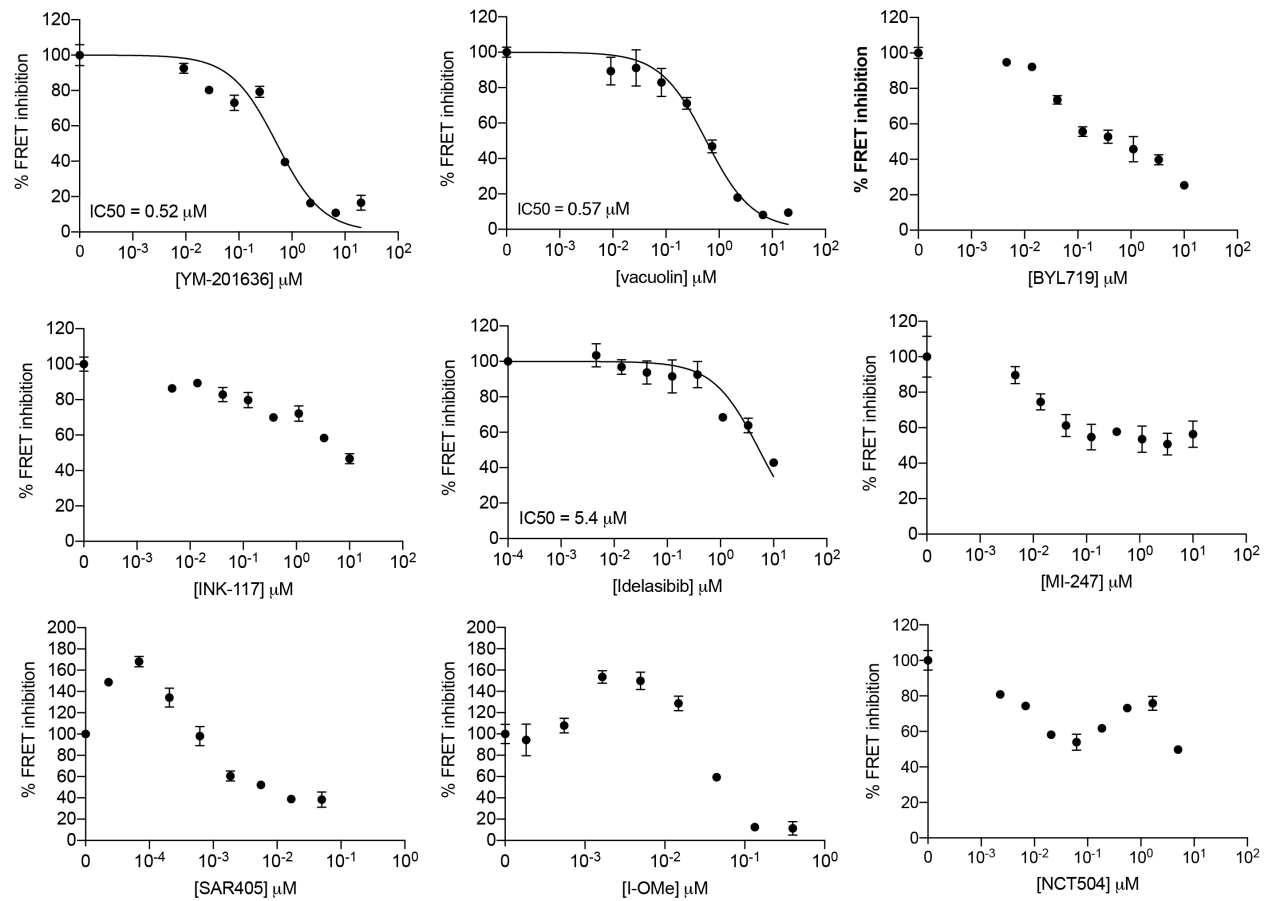
753
754
755

Fig. S2. Aggregation efficiency in FRET reporter cells treated with various concentration of inhibitors of phosphatidylinositol signaling pathway members. Error bars represent mean ± s.e.m from n = 3 technical replicates.

27

767 **SUPPLEMENTAL TABLE LEGENDS:**
768

769 **Table S1: Phenotypes and p-values from the primary CRISPRi genome-wide screen for**
770 **genes controlling α-synuclein aggregation.**
771 Whole Genome tab: Results from CRISPRi screens for were analyzed by the MAGeCK-iNC
772 pipeline (see Methods for details) and are listed for all genes in the genome. In order to compare
773 phenotypes between sublibraries screened on different days, phenotypes for each sgRNA within
774 each sublibrary were normalized to the standard deviation of non-targeting control within each
775 screen Columns are: Targeted transcription start site, knockdown phenotype (epsilon), P value,
776 and Gene score.
777 Hits tab: Hit genes determined using an FDR<0.05 and their categorization for visualization in
778 **Fig. 1B**. Columns are: Targeted transcription start site, knockdown phenotype (epsilon), P value,
779 and Gene score, Gene categorization.
780

781 **Table S2: sgRNA protospacer sequences and phenotypes from focused CRISPRi retest**
782 **screens, individually cloned sgRNA, their knockdown efficiency by qPCR, and qPCR**
783 **primer sequences.**
784 Retest sgRNA tab: Protospacer sequences of the focused retest library shown in **Fig. 2**.
785 Retest clustering results tab: Relative phenotypes from focused screen in **Fig 2B**.
786 sgRNA oligos and qPCR tab: Oligonucleotide sequences used to clone sgRNAs and their
787 knockdown efficiencies by qPCR.
788 qPCR primers tab: Oligonucleotide sequences used for qPCR experiments.
789